Presence of silver in the strengthening particles of an Al-Cu-Mg-Si-Zr-Ti-Ag alloy during severe overaging and creep

Elisabetta Gariboldi[1a], Paola Bassani[2], Mihaela Albu[3], Ferdinand Hofer[4]

ABSTRACT

The results of a study aimed at investigating the presence of silver in the strengthening phases of age-hardenable AlCuMgSi alloys are presented. HR STEM observations were performed on Al-4Cu-0.55Mg-0.5Si-0.5Ag-0.15Zr-0.1Ti (wt%) alloy samples aged or crept at 200°C to monitor the evolution of secondary phases over long times. Results showed that in the peak aged condition silver mostly segregated at the surface of some strengthening precipitates types. This occurred specifically at the plate-shaped particle/matrix interface of θ' phase while plate-like shaped particles, matching the wide compositional range of the quaternary Q' phase were free from Ag. A third population of strengthening particles was also observed, in the shape of core-shell rods. They were characterized by a Mg- and Si-rich core and a Cu-rich and Ag-rich shell. The exposure at 200 °C for up to 570 h, caused an evident coarsening of Q' and θ' plate-like particles, and the Ag surface enrichment of the latter went progressively lost. On the contrary, silver concentrated in small surface portions on the core-shell particles for which a relatively low coarsening rate was observed.

KEYWORDS

[1] Politecnico di Milano, Dipartimento di Meccanica, Via La Masa 1, 20156 Milano, Italy

[2] CNR ICMATE Institute of Condensed Matter Chemistry and Technologies for Energy. C.so Promessi Sposi 29, 23900 Lecco (Italy). Paola.bassani@cnr.it

[3] Graz Center for Electron Microscopy (ZFE), Steyrergasse 17/III, A-8010 Graz, Austria

[4] Institute for Electron Microscopy and Nanoanalysis, Graz University of Technology. Steyrergasse 17/III, A-8010 Graz, Austria

Aluminium alloys, electron microscopy, microanalyses, aging, precipitation.

INTRODUCTION

During service at high temperature Al age–hardenable alloys display overaging effects that affect long-term properties such as creep resistance. Thus, the microstructural modifications taking place under these conditions should be investigated in detail. Addition of silver was reported [1-8] to improve the high-temperature behavior of different Al-alloys. This effect has been related to the interaction of Ag with secondary phases that are present in these alloys, rather than to solid solution effects. Literature studies performed on alloys up to peak aged condition suggest three different scenarios (not necessarily alternative): i) the particle nucleation-enhancement [3, 4, 9], ii) the appearance of Ag in the structure of secondary phases and iii) the segregation of Ag at specific particle/matrix interfaces.

In some cases the presence of Ag led to formation of completely new phases as far as composition and crystal structure are concerned (as for example γ' ($AlAg_2$) [6]). In other cases the composition and/or structure of the Ag-bearing phases were similar to those of the 'conventional' precipitates as for example the X' ($Al_2CuMg(Ag)$), hexagonal phase with chemical composition similar to the common S phase [3].

In Al-Cu-Mg-Si alloys in which Ω phase forms, segregation of Ag at particle/matrix interfaces was observed. Ω phase has a chemical composition close to that of ϑ-Al_2Cu phase but nucleated over $\{111\}_\alpha$ planes from Mg-Ag clusters [3, 5, 7, 8]. A surface enrichment of Ag and Mg at the coherent interfaces of Ω particles, reduces the particle coarsening rate, with respect to that of ϑ' [3, 6, 8].

Less attention was devoted in literature to the evolution of the above mentioned particles beyond peak aging condition, when overaging appears. The beneficial effect of Ag addition to

[a]Corresponding author Email: elisabetta.gariboldi@polimi.it

Al-Cu-Mg alloy was found to abruptly decrease above 250 °C [3, 8]. Hutchinson [8] proposed a mechanism explaining Ω phase temperature-related coarsening rate on the basis of HRTEM observations and strain energy considerations. In another Al-Cu-Mg alloy tested at 200°C, Raviprasad [9] observed a reduction of Ω phase and increase of the more stable X' (Al_2CuMg(Ag)) phase, in which Ag was found inside the precipitate.

The effects brougth by Ag additions to commercial alloys of more complex composition, such as those based on Al-Cu-Mg-Si system, were also poorly investigated in the literature. It was observed that small addition of Si prevented Ω phase formation in Al-Cu-Mg-Ag alloys [10], while alternative phases (X, σ, θ, Q) with similar chemical composition were proposed for different element ratios in Al-Cu-Mg-Si-Ag alloys [9, 10]. The present paper targets the role of Ag on the microstructure behaviour over long exposure time at relatively high temperature of the Al-Cu-Mg-Si-Ag-Ti-Zr alloy, specifically on its effects on the strengthening particles. This alloy showed a higher overaging resistance and better creep strength when compared to an Ag-free alloy with similar amounts of the main alloying elements[11]. The strengthening phases formed at peak aging and their evolution have been monitored after exposure for more than 500 h at 200 °C.

EXPERIMENTAL

The investigated alloy had a nominal wt% composition of Al-4Cu-0.55Mg-0.5Si-0.5Ag-0.15Zr-0.1Ti (Al-1.75Cu-0.63Mg-0.49Si-0.13Ag-0.06Ti-0.05Zr at%) that was roughly confirmed by EDX analyses. It was cast in a cylinidrical mould of external diameter of 270 mm, and then sligthly axially compressed to reduce the amount of shrinkage pores. The cylinder, 180mm high, was supplied in T652 condition, consisting in solution treatment at about 500°C, water quenching, stress-releaving by compressive deformation at RT to about 2.5% plastic strain, and artificial ageing for 16 h at 160-165 °C.

The creep characterization of the alloy was carried out on cylindrical specimens sampled longitudinally or tangentially to the cylinder. Constant-load creep tests were performed at 150,

170 and 200°C for up to 2000 h to characterize the material high-temperature behaviour and their details were given elsewhere [11, 12]. The microstructural stability of the alloy was investigated at 200 °C, where the most severe overaging was expected to, by means of Vickers hardness, ligth optical, SEM and TEM observations. These analyses were carried out on samples transversally cut both from the external part of gripping ends and in the region of homogeneous strain within the specimen gauge length. The first samples were considered as representative for the material just aged at high temperature and the '-ag' suffix was used for their identification. The second set of samples were representative for the material additionally crept and '-cr' suffix used in these cases. A set of 5 Vickers hardness indentations with applied load of 0.49 N were performed on each sample gripping end or gauge length, after its conventional metallographic preparation. A reduced set of 4 samples crept at 200 °C for different times was selected for TEM investigations.

These specimens were prepared by electro polishing and/or Ar ions-milling using a Precision Ion Polishing System (PIPS, Gatan Inc.) at a voltage of 4 kV with incident angles of the ion cannons of 6° and 4° until perforation of the sample happened. Most of the sample prepared by electro polishing were then shortly post treated with PIPS.

High resolution STEM investigations were performed on a probe corrected FEI Titan G2 60–300 (S/TEM) microscope with an X-FEG Schottky field-emission electron source operated at 300 kV (current of 150 pA, beam diamater of 1Å). The microscope is equipped with a FEI Super-X detector (Chemi-STEM technology), consisting of four separate silicon drift detectors [13] and a Dual EELS - Gatan Imaging Filter (GIF) Quantum [14]. High Angular Annular Dark Field (HAADF) and Annular Dark Field (ADF) detectors were used to acquire micrographs.

For better imaging condition of the nano-sized phases at atomic resolution, the specimens were oriented (when possible) along the $<100>_{\alpha}$, $<110>_{\alpha}$ and $<112>_{\alpha}$ directions of the aluminum matrix.

Analytical investigations were done by X-ray spectroscopy using the k-factor method [15] for elemental quantification. Sample thickness in different areas was checked by Electron Energy

Loss Spectroscopy (EELS) [16], using an electron inelastic mean free path (EIMFP) of λ = 131 nm.

Intragranular particle lenght was measured on micrographs taken in sample regions of thickness ranging from 35 to 75 nm, oriented along $[100]_\alpha$. In order to get a relatively high number of particles as well as a good resolution of the smallest ones, micrographs at two different magnifications were used for the samples characterized by short and long exposure time at 200 °C. The sampled area was of about 0.2 μm^2 in the first case, 1.3 μm^2 in the latter.

Additionally, lower magnification images were acquired with a FEG-SEM system (SU-70 Hitachi) operated in transmission mode, for general overview of particles distribution.

RESULTS

In the as received condition, optical micrographs revealed radially elongated grains and coarse secondary phases at their boundaries. These were mainly θ-Al_2Cu particles, while other had a composition close to $Al_4Cu_2Mg_8Si_7$ of Q phase [17].

The hardness of samples aged and crept at 200°C is presented in Figure 1a and 1b, respectively. A marked reduction in hardness can be observed, the effect being higher in the crept than in aged samples. The same figures show the significant hardness differences of the (labelled) conditions from which the 8 STEM samples were obtained.

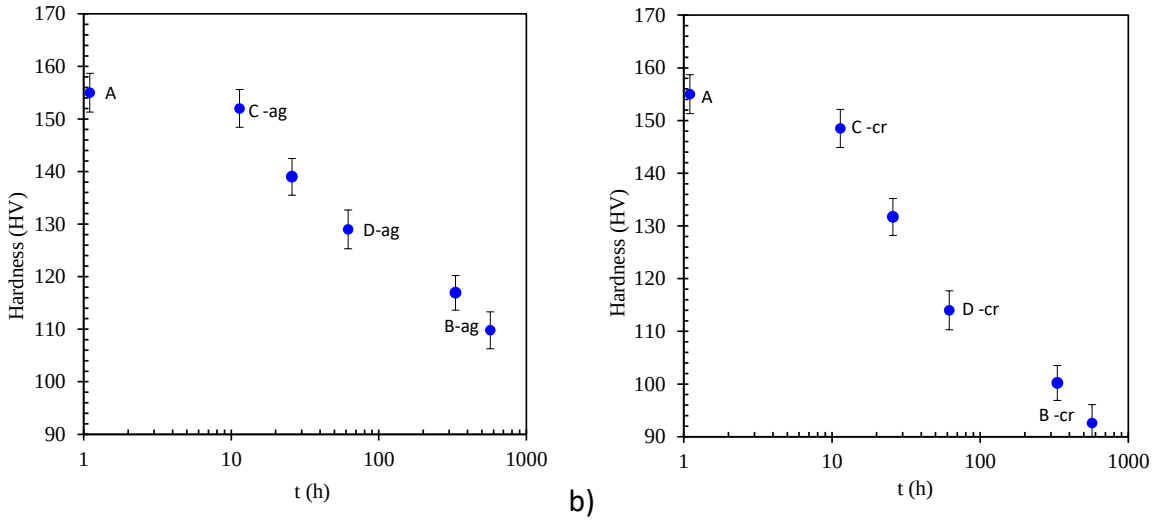

a) b)

Fig 1

Low-magnification STEM analyses of all samples revealed, in addition to the particles observed with optical microscopy, other dispersoids up to 200 nm, that were located close to grain boundaries. Most of these dispersoids were of Mn-Si-Cu-Fe, Fe-Mn-Si or were rich in Zr and/or Si together with, Cu, Mn, Mg in minor amounts (such as those clearly visible in Figure 2). Some of the remaining were Al-Cu-Ag phases with 6 to 9 Cu/Ag atomic ratio. The composition, density as well as the size of dispersoids did not significantly change during exposure at high temperature.

No silver was detected in the α phase matrix, as suggested by Al-Ag phase diagrams [18]. EDX analyses revealed also the absence of Si and Cu and the presence of Mg within the solubility limits at 200°C [19-21].

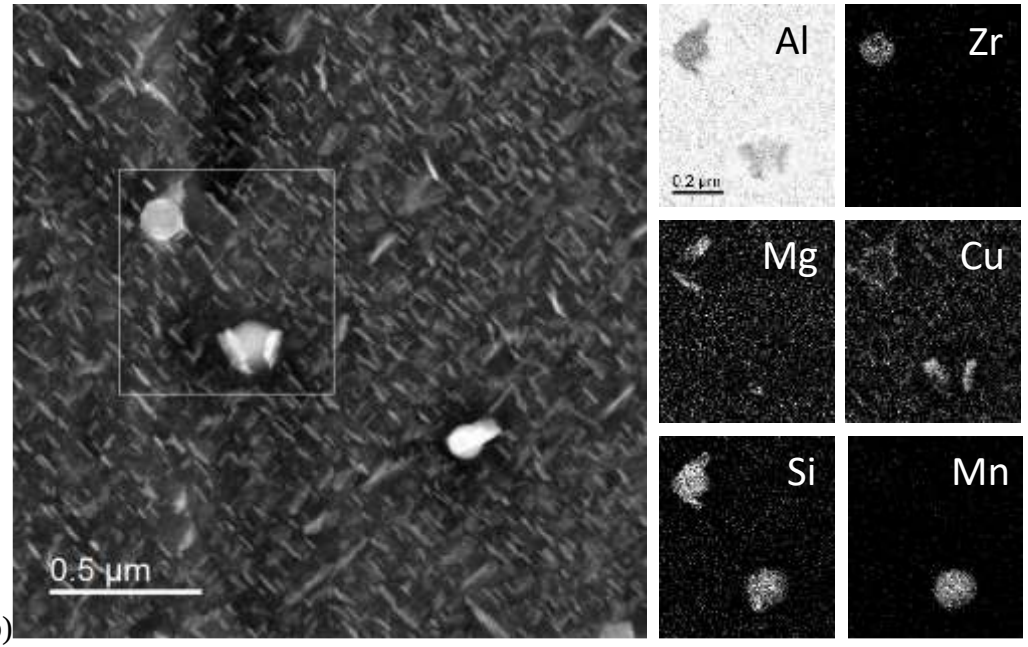

b) Fig 2

Also typical intragranular microstructure characterized by the presence of finer, strengthening particles was observed in Figure 2, as well as in Figure 3. The intragranular particles size significantly evolved during long-term aging or creep time at 200°C. (Figure 3). The cumulative distribution of intragranular particle length is illustrated in Figure 4a and 4b for

aged and crept samples, respectively, considering 10 nm intervals. In the peak aged condition, more than 25% of particles were in the smaller size range, i.e (smaller than 10 nm). Interestingly, in the most overaged aged and crept samples, 50% of the particles are still in a size range below 50 nm.

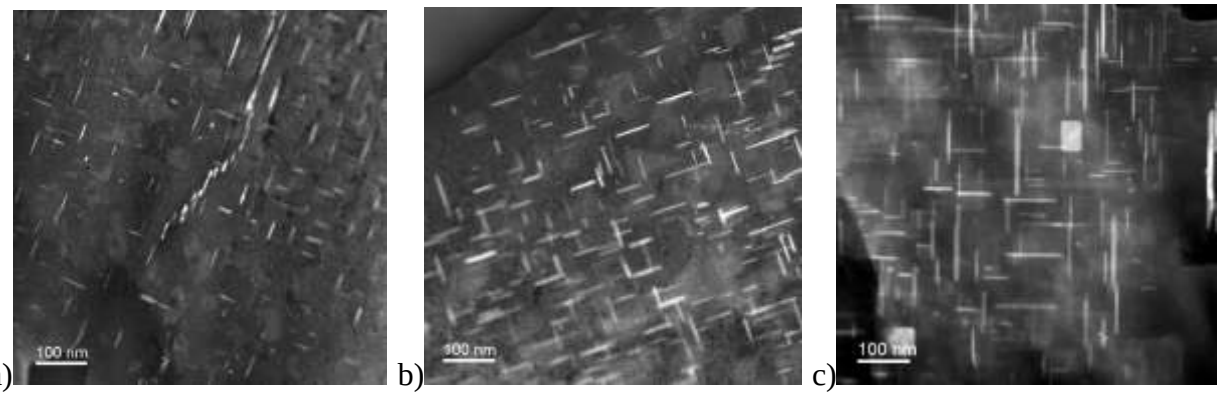

a) b) c)

Fig 3

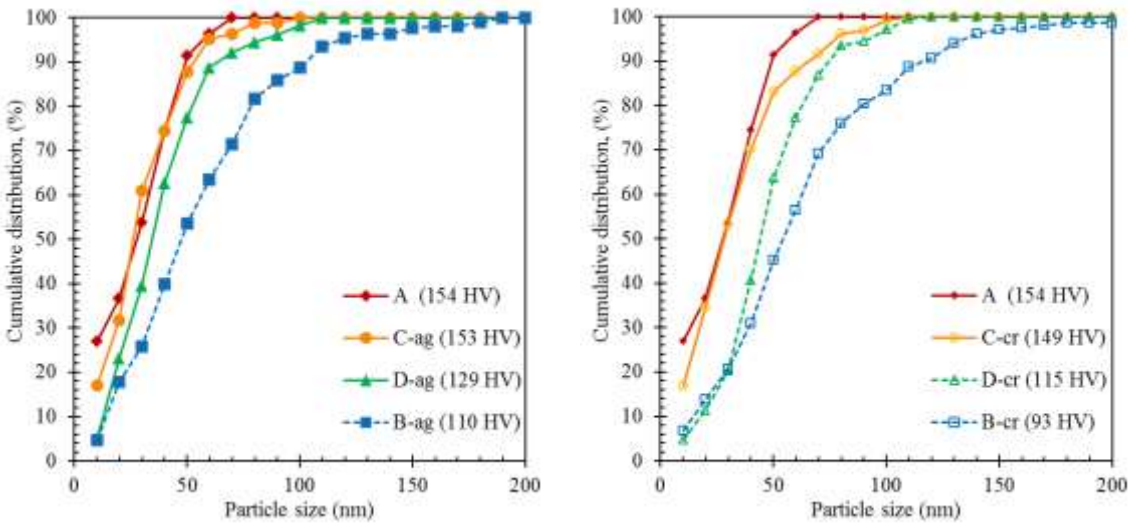

Fig.4

At higher TEM magnifications, the strenthening particles can be grouped in three different populations, among which the expected plate-shaped θ' particles, of θ-Al_2Cu precipitation sequence. The crystal structure of θ' is distinct from α-Al, with orientation relationship $((001)_{\theta'}//(001)_{\alpha}$, $[100]_{\theta'}//[100]_{\alpha}$ and coherence along the $<100>_{\theta'}$ directions [22]. In the A, C-ag and C-cr specimens, the size of the particles, in relatively high amount, was of the order of

tens of nanometers, and their thickness of some nanometers. Z-contrast in HAADF images (scaled with $Z^{1.7}$) of these particles confirmed their layered structure and, at the same time, revealed an outer layer of stronger Z-contrast (Figure 5a,) at the wide coherent particle/matrix interface.

The X-ray line profile analyses performed on these particles (Figures 5b), confirmed the presence of Cu-rich layers in the particle bulk and Ag mainly segregated in the outer 0.5 nm (2-3 monolayers of Ag) of the planar interfaces. The end portions of the particles were characterized by lower Z contrast, suggesting no Ag segregation there. It has to be noted that the matrix and particle in Figure 5a are slightly off the [110] zone axis.

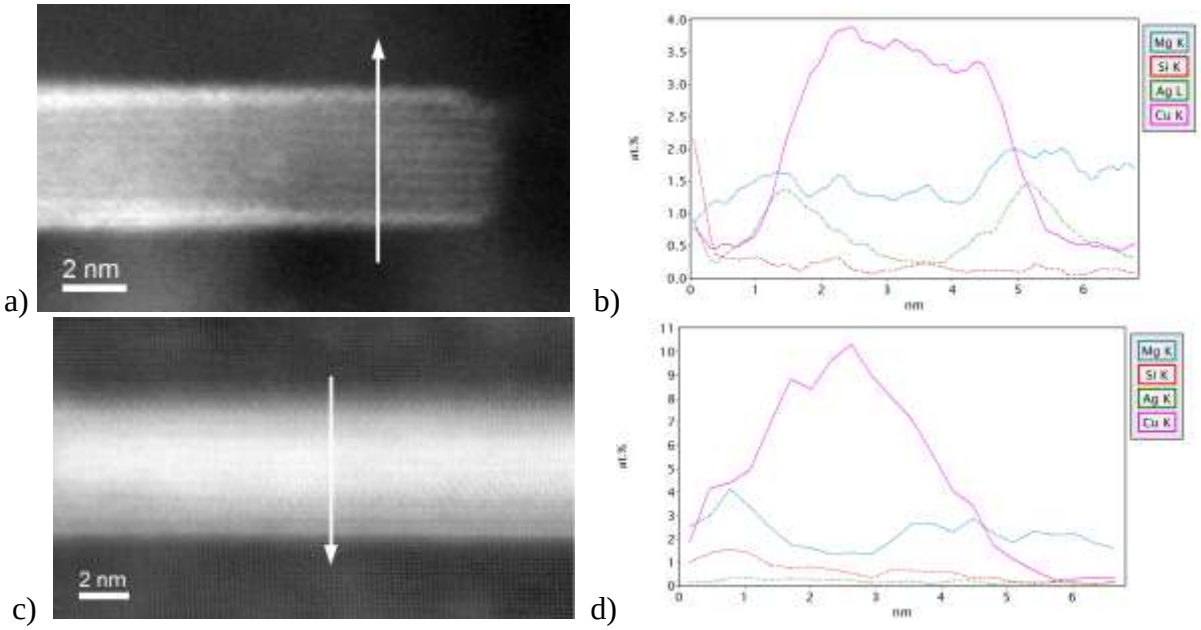

Fig.5

As exposure time at 200°C increased, this population of particles having plate-like morphology coarsened reaching up to 200 nm, while their thickness remained less than 8-10 nm. Further, the presence of silver on the outer surface of θ' particles decreased and became negligible in samples aged or crept for more than 60 hours at 200°C, while Mg was sometimes observed to increase in the same region (Figure 5c and 5d,).

The STEM EDX analysis in Figure 5d indicated a concentration of Al-1.4Mg-0.24Ag-0.7Si-9.5Cu- (at%) in the center of the particle and Al-3.5Mg-0.25Ag-1.43Si-4.48Cu (at%) at the upper interface with the matrix in Figure 5c. The specimen crept for the longest time at 200°C presented some coarse and almost squared particles (Figure 3c). High resolution observations revealed semicoherency with the matrix, indication of their evolution toward the stable θ phase. A second population of homogeneous plate-shaped particles of some tens of nm in length, in small amount, was characterized by relatively higher content of Al, Mg, Si and by lower content of Cu. The average composition corresponded to the relatively wide range presented in literature for Q phase and his precursors, typically of rod/needle or lath morphology [17, 23]. These precipitates were here referred as metastable Q' particles, also on the basis of a previous DSC study carried out on the same material in various temper conditions [24]. When alignment was along $<001>_{\alpha}$, Z-contrast suggested layered structure easily distinguishable from θ' and corresponding to that proposed in literature[25]. Profile microanalyses confirmed the presence of Mg, Si and of relatively low Cu. No Ag in the bulk nor Ag-enrichment at particle/matrix interface was clearly revealed by profile microanalyses, even if in all investigated samples, an outer layer of slightly stronger Z-contrast with respect to the bulk structure was sometime observed, such as in the example from specimen B-cr shown in Figure 6.

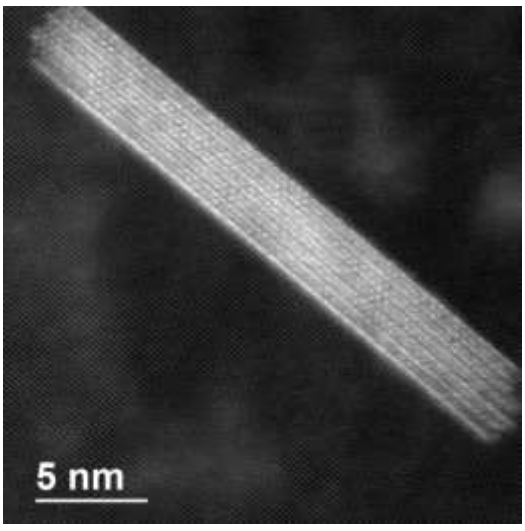

Figure 6

A third population of intragranular particles consisting of smaller particles, in a relatively high number per unit volume was found in the as-received condition (Figure 7a). They have a rod-

like shape with main axis aligned to <001>$_\alpha$ directions. Moreover, Z-contrast HAADF images of their cross sections acquired with the matrix tilted in the <001>$_\alpha$ zone axes, revealed a core-shell structure, with brighter external shell. Particles of this third population will thus be hereafter referred as core-shell ones. X-ray analyses in the as-received condition indicated the presence of Cu and Ag mainly in the shell with a ratio of about 3:1, while the core is reach in Si and Mg with a Mg:Si ratio of 1.5 or higher. In the peak aged sample A, the typical size of their cross sections was of 2-4 nm (Figure 7a) while their length extend to tens of nanometers.

a) 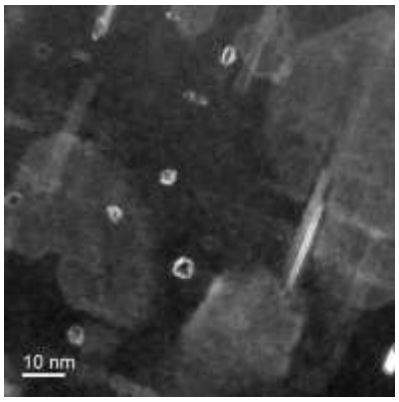

b) 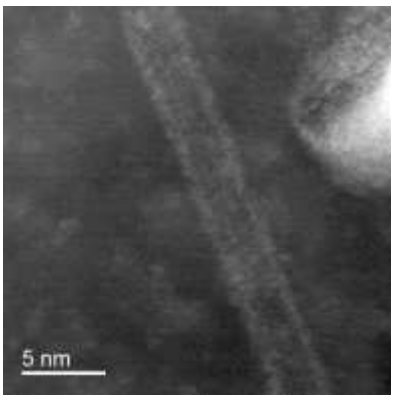

Fig 7

Figure 7. Representative features of core-shell rod-like particles a) Relative high amount of the fine particles in sample A (viewed along the [110] zone axis). b) Longitudinal view of core-shell rod-shape particle in the same sample D-ag (viewed along the [112] zone axis).

Qualitative estimation of the density of core-shell rod-shaped particles from micrographs suggested that it decreased in samples aged or crept at 200°C for longer times (Figure 3). Further, they tended to grow along <100>$_\alpha$ direction, their coarsening being in any case slower compared to the other two populations. The particle cross section size exceeded 15 nm only in exceptional cases. Interface Ag- or Cu-rich distribution was rather regular in smaller particles, characterized by nearly round or rectangular sections, whilst the distribution was not even for bigger particles, sometimes also displaying irregular shape, as exemplified in Figures 8a and 8f.

The rods showed a low Z-contrast in the [112] zone axis which display them in their length (see Figure 7b), therefore it was difficult to estimate their aspect ratio and qualitatively evaluate their possible lengthening during aging.

a) 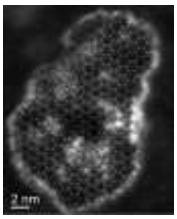 b) 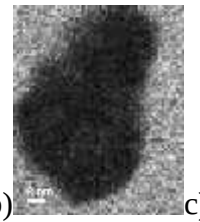 c) 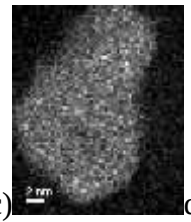 d) 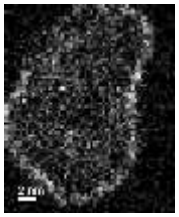 e) 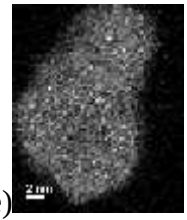 f) 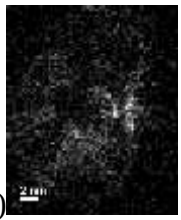
Fig8

In addition to the above populations of homogeneous particles, many interacting or aggregated particles were observed. These structures were found in all the investigated samples, in lower amount and generally with simpler structure for short exposure at 200°C.

Among coprecipitates, layered particles formed by θ'+ Q' phases as alternate structure were frequently observed in peak aged or shortly aged samples. Z contrast in HAADF micrographs suggested θ' as brighter regions (Figures 9a, 9c), the compositional profile confirming the phases chemistry (as in Figure 9b). The darker region of the particle in Figure 9a and 9c was identified by the EDX line scans to be Q' (Figure 9b). Local chemical composition of these layered, plate-like coprecipitates revealed chemical changes within the same particle population and even compositional shifts within the same particle. No significant enrichment of Ag was noticed at phase interface.

Other types of interacting phases observed in overaged samples involve core shell rods and θ' or Q' phases. In these co-precipitates the evolved core-shell particles protruded at ends of some θ' particles (Figure 9d) or decorated the extended surfaces of θ' or Q' phases. Silver was often found here at the surface of the core-shell phase.

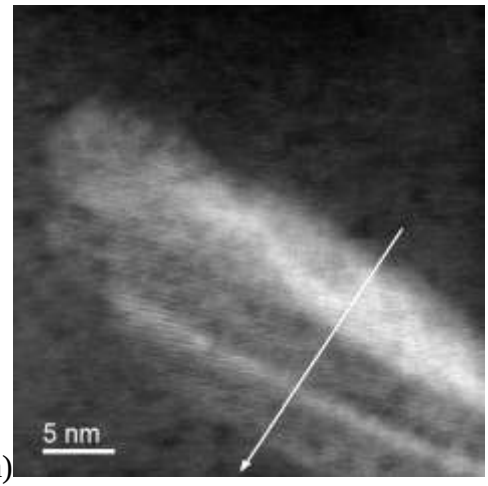

a)

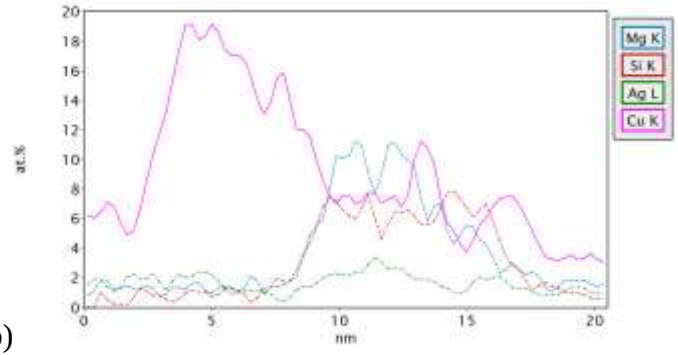

b)

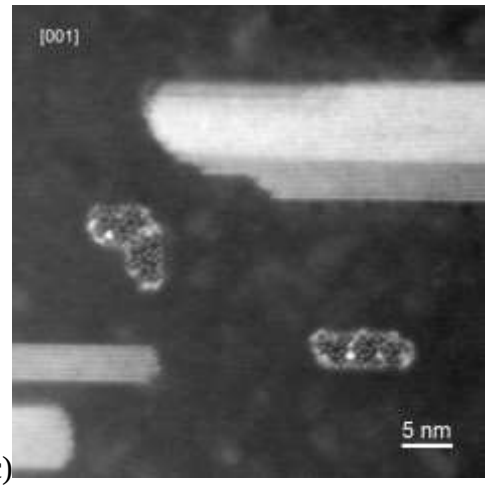

c)

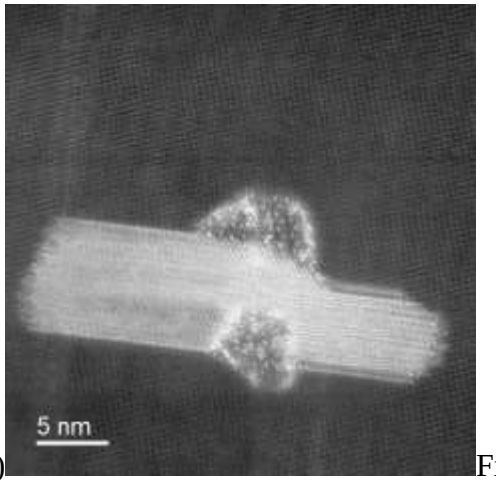

d) Fig 9

DISCUSSION

Among the three populations of homogeneous particles and coprecipitates, only θ’ particles could be clearly identified, having a well-defined chemical composition. Literature survey showed a wide range of particles referred as Q’ precursors (Q_P, Q_C, L and C phase), characterized by slightly different composition, but also with different morphology, both related to alloy composition and aging temperature [17, 23, 25-28]. Even if an exact match could not be found, both Q’ and core-shell were compatible to such precursors. As a matter of fact, the chemical composition of core-shell particles could not actually match those proposed in literature for other phases such as S (Al_2CuMg), β (Mg_2Si), X’ ($Al_2CuMgAg$) [3, 9, 28]. The exact structural characterization of these two particles populations was out of the scope of the present paper.

The microstructural investigations showed that, even if the silver additions (0.13 at%) was relatively low, it played an important role in the type and development of the second phases. Only a small amount of this alloying element was included in relatively coarse dispersoids at grain boundaries. The remaining was only found at some particle/matrix interfaces.

The θ' particles, in the sample A (peak aged at 160-165°C), had coherent flat particle/matrix surfaces enriched with silver, and this enrichment was kept only for short exposure times at 200°C (sample C-ag). Starting from sample D-ag, a clear reduction of silver at interface was observed and eventually was completely absent at longer exposure times (sample B-cr). This change correlates very well to hardness reduction. This situation was compatible both to a reduced stability of the outer Ag- rich layer at 200°C compared to 160-165°C and to an insufficient Ag flow through the matrix. On the other hand, it was fundamentally different from what observed by Rosalie et al. [6] since their alloy was much richer in silver. In another investigation done by Ohno et al. [5] in Al–1.9Cu–0.3Mg–0.2Ag alloy (composition in at %) aged at 180°C the formation of Ω phase prevented the Ag segregation at θ'/particle interface.

Also core shell particle showed surface Ag enrichment. In the as-received condition they were mostly of round cross section and characterized by the presence of an outer layer with higher Ag and Cu amounts than their inner part, this latter richer in Mg, Si and Al. During overaging the morphology of the cross-section progressively evolved from round to irregular appearing wider in $<100>_{\alpha}$, with aspect ratios not exceeding 2:1. At the same time the Ag surface layer of these particles loose continuity with increasing time exposure and Ag segregation was partly replaced by Cu. Something similar occurred also in interacting coprecipitates in which core shell phase is involved.

Layered coprecipitates ccould have been favoured by the change of aging temperature that modified the equilibrium composition of Q' phase, leading to the formation of new Q' phase of different composition. During long-time exposure interdiffusion of elements took place and induced homogenization of these particles transforming them in Q or θ'+core shell particles.

Interacting coprecipitates can be also interpreted as an evolution of theta θ' particles: as the amount of Ag segregated at the particle/matrix interface of θ' phase reduces, the formation of a surface layer containing Mg, Si and Cu can lead to the nucleation of core-shell similar particles (Figure 9d). In order to clarify those modifications, atomic and molecular dynamic simulations are needed.

The amount of the abovementioned particle populations seemed not to be affected by the applied stress, but their evolution was strongly accelerated. Comparing aged to crept samples, no qualitative difference of type of particles could be appreciated. Also Ag localization was the same in the two groups of observed samples. On the other hand, the coarsening, especially of the plate-like particles was faster. In fact for aged samples the distribution of particle length increased constantly while for the crept ones in the low-size region remained approximately unchanged, but above approximately 30 nm their coarsening rate was shifted towards higher values. This is reasonably due to stress-enhanced diffusion.

CONCLUSIONS

The following conclusions can be derived from the research study carried out on Al-4Cu-0.55Mg-0.5Si-0.5Ag-0.15Zr-0.1Ti alloy in differently aged or crept conditions.

- The alloy showed the presence of three populations of strengthening phases: θ', plate Q' and particles referred as core/shell rods, as well as two types of co-precipitates. The first two groups and their co-precipitates are widely known in literature. Core-shell particles could be assigned to rod-shaped Q precursors family, according to EDS analyses: nevertheless they deserve more careful investigation, especially as far as their crystal structure is concerned.
- Only small part of the silver in the alloy concurred to the formation of dispersoids. Most Ag was found at the θ' and core/shell particle/matrix interface, while Q' plate-like particles did not show a clear enrichment of this element.

- During exposure at 200 C°, a rather monotonous change in size and distribution of both plate-like and core-shell particles was qualitatively observed, even if to a different extent, and it was consistent with the progressive material softening, which was stress-enhanced in crept specimens. A reduction of individual (separate) core-shell rods particles as well as an increase of co-precipitates number and type was noticed. Also Ag distribution changed: its segregation at particles surfaces progressively reduced and, after long-term exposure at 200°C, only the core-shell rods and their coprecipitates presented some Ag enrichment. The Ag-rich surface layer was not continuous, but instead localized Ag-rich spots within a Cu-rich surface layer were observed, with reduced efficiency as diffusion barrier. Core shell precipitates were characterized by relatively low coarsening rate.

AKNOWLEDGMENTS

The research leading to these results has received funding from the European Union Seventh Framework Programme under Grant Agreement 312483 - ESTEEM2 (Integrated Infrastructure Initiative–I3).

REFERENCES

1) I.J. Polmear, Aluminium alloys – A century of age hardening, Mater. Forum 28 (2004) 1-14.
2) J.S. Robinson, R.L. Cudd, J.T. Rvans, Creep resistant aluminium alloys and their Applications, Mater. Sci. Techn. 19 (2003) 143-155.
3) P. Ringer, K. Hono, Microstructural Evolution and Age Hardening in Aluminium Alloys: Atom Probe Field-Ion Microscopy and Transmission Electron Microscopy Studies, Mater. Character. 44 (2000) 101–131.

4) X. Zhou, L. Zhayi, S. Bai, M. Liu, P. Ying, The influence of various Ag additions on the nucleation and thermal stability of Ω phase in Al-Cu-Mg alloys, Mater. Sci. Eng. A564 (2013) 186-191.

5) K. Hono, Nanoscale microstructural analysis of metallic materials by atom probe field ion microscopy, Progr. Mater. Sci. 47 (2002) 621-729.

6) J.M. Rosalie, L. Bourgeois, Silver segregation to θ'(Al2Cu)–Al interfaces in Al–Cu–Ag alloys, Acta Mater. 60 (2012) 6033-6041.

7) D. Bakavos, P.B. Prangnell, B. Bes, F. Eberl, The effect of silver on microstructural evolution in two 2xxx series Al-alloys with a high Cu:Mg ratio during ageing to a T8 temper, Mater. Sci. Eng. A491 (2008) 214-223.

8) C.R. Hutchinson, X. Fan, S.J. Pennycook, G.J. Shiflet, On the origin of the high coarsening resistance of Ω plates in Al-Cu-Mg-Ag alloys, Acta Mater. 49 (2001) 2827-2841.

9) K. Raviprasad, C.R. Hutchinson, T. Sakurai, S.P. Ringer, Precipitation processes in an Al-2.5Cu-1.5Mg (wt%) alloy microalloyed with Ag and Si. Acta Mater. 51 (2003) 5037-5050.

10) D.G. Eskin, Decomposition of supersaturated solid solutions in Al–Cu–Mg–Si alloys, J. Mater. Sci. 38 (2003) 279-290.

11) E. Gariboldi. Effect of prior aging on the creep properties of 2xxx age-hardenable alloys. Proc. ECCC Conference 2014, Rome. (ISBN 9788874843800).

12) E. Gariboldi, A. Lo Conte, Effects of orientation and overaging on the creep and creep crack growth properties of 2xxx aluminium alloy forgings. In H. Altenbach , S. Krauch (Eds), Advanced Materials Modelling for structures, Springer, 2013, pp 165-177.

13) P. Schlossmacher, D.O. Klenov, B. Freitag, H.S. von Harrach, Enhanced Detection Sensitivity with a New Windowless XEDS System for AEM Based on Silicon Drift Detector Technology, Microscopy Today 18 (2010) 14–20.

14) A. Gubbens, M. Barfels, C. Trevor, R. Twesten, P. Mooney, P. Thomas, N. Menon, B. Kraus, C. Mao and B. McGinn, The GIF Quantum, a next generation post-column imaging energy filter. Ultramicroscopy 110 (2010) 962–970.

15) J.I. Goldstein, D.B. Williams, G. Cliff, Quantification of energy dispersive spectra,: in: D.C. Joy, A.D. Romig, J.L. Goldstein (Eds), Principles of Analytical Electron Microscopy, , Plenum Press, New York, 1986, pp 155-217.

16) R.F. Egerton, TEM Applications of EELS in Electron Energy-Loss Spectroscopy in the Electron Microscope, Spinger, 1996, pp. 293.

17) D.J. Chakrabarti, D.E. Lauglin, Phase relations and precipitation in Al-Mg-Si alloys with Cu additions, Progr. Mat. Sci. 49 (2004) 389-410.

18) V.T. Witusiewicz, U. Hecht, S.G. Fries, S. Rex, The Ag–Al–Cu system: Part I: Reassessment of the constituent binaries on the basis of new experimental data. J. Alloys Comp.385 (2004) 133-143.

19) J.L. Murray, J.A. McAlister, The Al-Si (Aluminium-Silicon) System. Bulletin of Alloy Phase Diagr. 5 (1984) 74-84.

20) T.B. Massalsky, The Al-Cu (Aluminium-Cupper) System. Bull. Alloy Phase Diagr. 1 (1980) 27-33.

21) J.L. Murray, The Al-Mg (Aluminium-Magnesium) System. Bull. Alloy Phase Diagr. 3 (1982) 60-74.

22) L. Bourgeois, C. Dwyer, M. Weyland, J-F Nie, B.C. Muddle, The magic thicknesses of θ‘ precipitates in Sn-microalloyed Al–Cu, Acta Mater. 60 (2012) 633–644.

23) A. Biswas, D.J. Siegel, D.N. Seidman, Compositional evolution of Q-phase precipitates in an Al alloy, Acta Mater.. 75 (2014) 322-326.

24) P. Bassani, E. Gariboldi, D. Ripamonti, Thermal analysis of Al-Cu-Mg-Si alloy with Ag/Zr additions, J. Therm.l Anal. Calorim. 91 (2008) 29–35.

25) K. Matsuda, D. Teguri, T. Sato, Y. Uetani, S. Ikeno. Cu segregation around Metastable Phases in Al-Mg-Si alloy with Cu. Mater. Trans. 46 (2007) 967-974.

26) C. D. Marioara, S. J. Andersen, T. N. Stene , H. Hasting , J. Walmsley, A.T.J. Van Helvoort & R. Holmestad, The effect of Cu on precipitation in Al–Mg–Si alloys. Phil. Mag. 87 (2007) 3385–3413.

27) S, Wenner, C.D.l Marioara, S.J. Andersen, M. E. Ervik, R. Holmestad, A hybrid aluminium alloy and its zoo of interacting nano-precipitates, , NorwayMaterials Characterization 106 (2015) 226–231.

28) M. Torsaeter, W. Lefebvre, C.D. Marioara, S.J. Andersen, J.C. Walmsley, R. Holmestad, Study of intergrown L and Q' precipitates in Al–Mg–Si–Cu alloys. Scripta Materialia 64 (2011) 817–820.

FIGURE CAPTIONS

Figure 1. Vickers hardness of specimens creep tested at 200°C as function of creep rupture times, up to 570 h. Specimens selected for TEM analyses are labelled. Sample A, here indicated in both graphs at time of 1h, represents the as-received condition. Indentations were performed on gripping ends (a) and on the gauge length of creep specimens (b). Bars refer to standard deviation.

Figure 2. Representative STEM HAADF micrographs of inhomogeneous dispersoids and their elemental distribution obtained by EDS mapping in as received specimen A.

Figure 3. STEM HAADF micrographs and corresponding particle size distribution showing the evolution of intragranular particle distribution in samples in different aging or creep condition: a) sample A, b) D-ag, c) B-cr.

Figure 4. Cumulative distribution of intragranular particle size of the STEM investigated aged (a) and crept (b) samples. For each sample the corresponding hardness is given. Dashed lines refer to measurements done on micrographs at lower magnification.

Figure 5. θ’ phase particles in different microstructural conditions (HAADF micrographs) and corresponding line profiles: a and b) sample C-cr, c and d) sample D-ag. In each profile, the correspondence of elements and lines is Cu-purple solid line, Ag-green dash-dot-dot line, Mg-blue dashed line, Si-red dash-dot line.

Figure 6. Plate-like Q’ phase particle in specimen B-cr.

Figure 7. Representative features of core-shell rod-like particles a) Relative high amount of the fine particles in sample A (viewed along the [011] zone axis). b) Longitudinal view of core-shell rod-shape particle in the same sample D-ag (viewed along the [112] zone axis).

Figure 8. Sample B-cr. HAADF image ([001] zone axis) of one of the particle identified as core-shell (a) and elemental distribution of Al (b), Mg (c), Cu (d), Si (e) and Ag (f) revealed by EDS probe. The average composition in the region of the particle gave (in at%) 38Mg-31Al-24Si-6Cu-1.1Ag.

Figure 9. Examples of inhomogeneous intragranular particles. a) HAADF micrograph (no specific orientation) of a layered particle of θ'+Q' phases in simple A. b) Corresponding line profile, where element-line correspondence is as in figure10a, c) STEM HAADF micrograph of precipitate particles observed in the sample B-cr crept for the longest time at 200°C, d) Phase with features similar to core-shell particles located at the edge of a θ' particle in D-cr sample ([001] zone axis).